



## Fractonic criticality in Rydberg atom arrays

Rafael A. Macêdo <sup>1</sup> and Rodrigo G. Pereira <sup>1,2</sup>

<sup>1</sup>*Departamento de Física Teórica e Experimental, Universidade Federal do Rio Grande do Norte, Natal, Rio Grande do Norte 59078-970, Brazil*

<sup>2</sup>*International Institute of Physics, Universidade Federal do Rio Grande do Norte, Natal, Rio Grande do Norte 59078-970, Brazil*



(Received 9 May 2024; revised 8 August 2024; accepted 8 August 2024; published 22 August 2024)

Fractonic matter can undergo unconventional phase transitions driven by the condensation of particles that move along subdimensional manifolds. We propose that this type of quantum critical point can be realized in a bilayer of crossed Rydberg chains. This system exhibits a transition between a disordered phase and a charge-density-wave phase with subextensive ground-state degeneracy. We show that this transition is described by a stack of critical Ising conformal field theories which become decoupled in the low-energy limit. We also analyze the transition using a Majorana mean-field approach for an effective lattice model, which confirms the picture of a fixed point of decoupled critical chains. We discuss the unusual scaling properties and derive anisotropic correlators that provide signatures of subdimensional criticality in this realistic setup.

DOI: [10.1103/PhysRevB.110.085144](https://doi.org/10.1103/PhysRevB.110.085144)

### I. INTRODUCTION

For decades, effective field theories have provided invaluable insight into quantum critical phenomena [1–4]. A general guiding principle is that the low-energy properties of a system close to a continuous phase transition are governed by nearly massless excitations. If these excitations propagate in all spatial directions, one expects universal scaling behavior once the correlation length diverges and microscopic details become irrelevant.

The standard continuum limit inherent in effective field theories has recently been challenged by the study of fracton phases of matter [5–7]. Fractonic systems are characterized by excitations that are completely immobile (fractons) or propagate along lower-dimensional subspaces (lineons and planons) [8–11]. In addition, fracton phases exhibit a subextensive ground-state degeneracy. These properties are associated with subsystem symmetries, which can be either exact or emergent [12–15] and play an important role in quantum phase transitions [16–20]. In particular, continuous transitions can be driven by the condensation of lineons and planons, leading to the notion of subdimensional criticality [19,20]. In this intriguing scenario, the transition is described by stacks of lower-dimensional critical theories, which decouple at low energies.

In continuum descriptions of fractons [21–30], physical observables often depend on a short length scale related to a lattice regularization. The need for this regularization becomes apparent in theories with higher spatial derivatives and anisotropic scaling, an early example of which was the Bose metal in 2+1 dimensions [31]; see also Ref. [32]. In this case, the dispersion  $\omega \sim k_x k_y$  of bosonic spin modes vanishes along lines in momentum space. As a consequence, high-momentum modes contribute to the low-energy physics, a phenomenon known as UV-IR mixing [15,27]. Similar theories have been proposed for the fracton critical point in a higher-order topological transition [33], the fractonic Berezinskii-Kosterlitz-Thouless transition in the

plaquette-dimer model [34,35], and boundaries of fracton models [36,37]. Crucially, UV-IR mixing imposes a modified renormalization group (RG) analysis [12,31,34,35,38–40]. In some contexts, the difficulties with scaling have been interpreted in terms of a dimensional reduction [12,38], whereby the two-dimensional (2D) model is viewed as an array of one-dimensional (1D) systems. Despite the enormous interest sparked by fractonlike physics, a major obstacle to its observation is that the proposed lattice models typically contain multispin interactions that are hard to realize experimentally.

In this work, we show that a fractonic transition can be observed in a realistic setup with Rydberg atom arrays, a versatile platform for the quantum simulation of long-sought phases of matter [41–49]. Our setup consists of two layers of parallel chains with two-body interactions only. In the limit of decoupled chains, each chain displays a transition between a  $\mathbb{Z}_2$ -ordered charge density wave (CDW) and a disordered phase [50,51]. The 1D critical point is described by the Ising conformal field theory (CFT). We consider the regime in which the leading interchain interaction occurs at the crossings between perpendicular chains, and its strength can be controlled by varying the layer separation. We first show that the ordered phase of the 2D array retains a subextensive ground-state degeneracy inherited from the spontaneous symmetry breaking of the individual chains. We refer to this phase as the fractonic CDW (fCDW). We analyze the transition from the fCDW to the disordered phase in terms of an array of Ising CFTs coupled at an extensive number of crossings. Using a RG approach, we find that the interlayer interaction in the effective (2+1)-dimensional theory behaves as a marginally irrelevant perturbation. As a result, the critical system displays 1D-like correlations. To confirm the nature of the critical point, we work out a Majorana mean-field theory for an effective lattice model. In this approach, the stability of the fixed point of decoupled chains is signaled by the absence of hybridization between Majorana modes in different chains at weak interchain coupling.

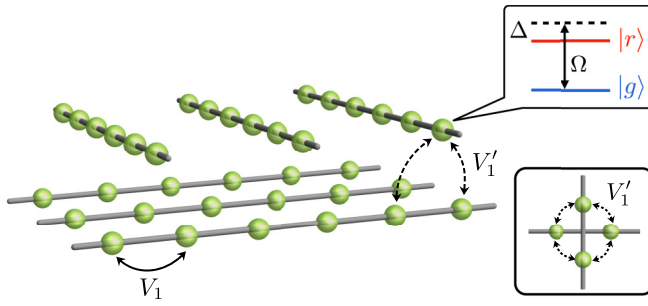


FIG. 1. Setup with Rydberg atoms placed in chains that belong to two different planes. The atoms are toggled between the ground state  $|g\rangle$  and a Rydberg state  $|r\rangle$  by the external Rabi frequency  $\Omega$  with a detuning  $\Delta$ . The leading interactions are the nearest-neighbor intra-chain coupling  $V_1$  and the interchain coupling  $V'_1$  around a crossing. The lower-right panel shows the top view of a single crossing.

This paper is organized as follows. In Sec. II, we present the lattice model and discuss the control parameters in the proposed setup. In Sec. III, we analyze the limiting cases of the model, describing the ground-state degeneracy and elementary excitations that characterize the fCDW phase. In Sec. IV we take the continuum limit and obtain the effective field theory for the fCDW-disorder transition. The Majorana mean-field theory that supports the conclusion of a decoupled-chain critical point is presented in Sec. V. We draw some conclusions in Sec. VI. Finally, details about the emergent symmetries in the continuum limit, the perturbative RG approach, and the self-consistent mean-field equations can be found in the Appendices.

## II. THE MODEL

We consider a model for  $N$  trapped Rydberg neutral atoms, which in general are described by the Hamiltonian [41,52]

$$H = \sum_{i=1}^N \left[ \frac{\Omega}{2} (b_i + b_i^\dagger) - \Delta n_i \right] + \sum_{1 \leq i < j \leq N} V_{ij} n_i n_j, \quad (1)$$

where  $b_i, b_i^\dagger$  are annihilation and creation operators for hard-core bosons for the  $i$ th atom, describing the ground state  $|g\rangle_i$  and the Rydberg state  $|r\rangle_i = b_i^\dagger |g\rangle_i$ , with  $n_i \equiv b_i^\dagger b_i$ . These states are coupled by external lasers with a Rabi frequency  $\Omega$  and a detuning  $\Delta > 0$ . The van der Waals interaction decays with the distance  $R_{ij}$  between atoms as  $V_{ij} = C_6 R_{ij}^{-6}$ , with a coefficient  $C_6 > 0$ .

The geometry of the lattice determines the leading interactions. In the setup of Fig. 1, the atoms are placed in 1D chains with lattice spacing  $a$ . Adjacent parallel chains are separated by a distance  $d_\perp = \nu a$ , with an integer  $\nu \geq 2$ , and the layers are separated by  $d_\perp$ . The shortest distance between perpendicular chains occurs at a ‘‘crossing’’ (as viewed from above) where each atom is coupled symmetrically to a pair of atoms in the other layer. This model respects a  $C_4$  lattice rotation symmetry, which also exchanges the layers, and a  $\mathbb{Z}_2$  time-reversal symmetry defined as complex conjugation. Due to the fast decay of the interactions, we consider only two terms,  $V_1$  and  $V'_1$ , corresponding to nearest-neighbor intrachain and interchain couplings, respectively. The ratio  $V'_1/V_1 = 8[1 +$

$2(d_\perp/a)^2]^{-3}$  varies rapidly with the layer separation. Importantly, we neglect direct couplings between parallel chains. In Fig. 1 and throughout this work, we represent the array with  $\nu = 2$  atoms between two crossings, but in practice it may be convenient to take  $\nu > 2$  to further suppress the interaction across the distance  $d_\perp$ .

We can map the Hamiltonian describing the interacting Rydberg atoms to a spin model by introducing the Pauli operators

$$Z_i = 2n_i - 1, \quad X_i = b_i + b_i^\dagger. \quad (2)$$

In particular, in the limit  $d_\perp \rightarrow \infty$  we can set  $V'_1 = 0$ , and the corresponding Hamiltonian  $H_0$  is equivalent to Ising chains with transverse and longitudinal fields [51]:

$$H_0 = \sum_{\ell=1}^{L_x+L_y} \sum_{m=1}^{L_\ell} (J Z_{m,\ell} Z_{m+1,\ell} + h_X X_{m,\ell} + h_Z Z_{m,\ell}), \quad (3)$$

where  $J = V_1/4 > 0$ ,  $h_X = \Omega/2$ , and  $h_Z = (V_1 - \Delta)/2$ . Here we have introduced a notation which is convenient for an array of spin chains:  $\ell$  is a chain index,  $m$  labels the position along the chain, and  $L_x$  ( $L_y$ ) is the number of vertical (horizontal) chains in the upper (lower) layer. To count the number of sites in each chain, we define  $L_\ell = \nu L_y$  for  $1 \leq \ell \leq L_x$  and  $L_\ell = \nu L_x$  for  $L_x + 1 \leq \ell \leq L_x + L_y$ . We also assume periodic boundary conditions. For finite  $d_\perp$ , the Hamiltonian in Eq. (3) is perturbed by the interchain coupling

$$\delta H = J' \sum_{\diamond} \sum_{(i,j) \in \diamond} Z_i Z_j, \quad (4)$$

where  $J' = V'_1/4 \geq 0$  and  $\diamond$  stands for the bonds around a crossing (see Fig. 1). In addition,  $V'_1$  renormalizes the longitudinal field by  $\delta h_Z = V'_1/2$ . Hereafter, we will discuss the model in terms of the spin variables and the parameters  $h_X$ ,  $h_Z$ ,  $J$ , and  $J'$ .

## III. PHASE DIAGRAM

First, let us discuss the limit of decoupled chains  $J' = 0$ , obtained by taking  $d_\perp \rightarrow \infty$ . The phase diagram of a single Ising chain has been studied numerically [53]. For sufficiently large  $h_X$  or  $h_Z$ , the system is in a trivial disordered phase. For  $h_X, h_Z \ll J$ , each chain locks into one of two CDW states represented by  $|\dots rgrg \dots\rangle$  or  $|\dots grgr \dots\rangle$ , breaking translational invariance. In particular, for  $h_Z = 0$  we recover the exactly solvable transverse-field Ising chain, for which the critical point is well known to occur at  $h_X/J = 1$ . More generally, a critical value of  $h_X/J$  exists provided that  $|h_Z| < J$ . In the ordered phase, each chain contributes with two states to the ground-state degeneracy, which implies a  $2^{L_x+L_y}$ -degenerate ground-state manifold in this limit.

To see the difference from a trivial stack of 1D states, we now turn on the interchain coupling  $J' > 0$ . In the following we shall assume that  $h_Z$  is fixed and discuss the phase diagram of the 2D model as a function of  $h_X/J$  and  $J'/J$ .

For  $h_X = 0$ , the Hamiltonian  $H = H_0 + \delta H$  reduces to a classical Ising model. For  $h_X = J' = 0$ , we have the  $2^{L_x+L_y}$  classical ground states with energy  $E_{\text{cl}}^{(1)} = -2\nu J L_x L_y$ . Note that this energy does not depend on  $J'$  due to the frustration of the interchain coupling. On the other hand, for  $h_X = 0$  and

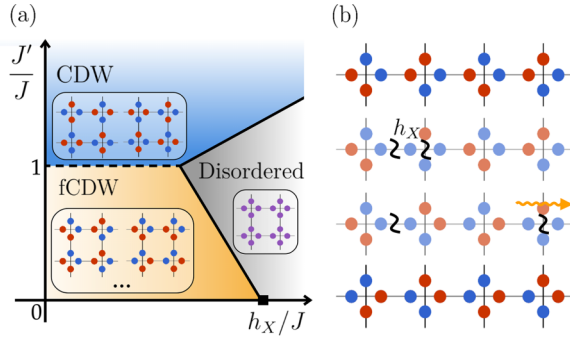


FIG. 2. (a) Schematic phase diagram for a fixed value of  $h_z \ll J$ . The local atomic states  $|g\rangle$  and  $|r\rangle$  in the ordered phases are represented by blue and red, respectively, while the disordered state is depicted in purple. The square on the  $J' = 0$  axis marks the critical point of decoupled chains. Solid (dashed) lines denote second-order (first-order) transitions. (b) Domain-wall excitations in the fCDW phase. Given an fCDW ground state (top), reaching another ground state (bottom) requires creating and moving domain walls around the system.

$J' \gg J$ , the classical ground state is only twofold degenerate, corresponding to CDW states in which the four atomic states around each crossing alternate as  $|rgrg\rangle$  or  $|grgr\rangle$  [see Fig. 2(a)]. These states have energy  $E_{\text{cl}}^{(2)} = -[4J' + 2(\nu - 2)J]L_x L_y$ . Therefore, increasing  $J'$  along the classical line in the phase diagram we encounter a level crossing at  $J' = J$ , associated with a first-order transition between the two types of ordered states.

One can go from the twofold-degenerate CDW to the disordered phase by increasing  $h_x$ . In the strong-coupling limit  $J'/J \gg 1$ , we can project the model onto the eigenstates  $|\tau^z = 1\rangle \equiv |rgrg\rangle$  and  $|\tau^z = -1\rangle \equiv |grgr\rangle$  of the interaction at each crossing. It is straightforward to show that the effective Hamiltonian in this limit is an Ising model (on the square lattice for  $\nu = 2$ ) with transverse field  $\tilde{h}_x \sim h_x^4/(J')^3$  at the projected sites. As expected from the spontaneous breaking of a global  $\mathbb{Z}_2$  symmetry, the transition from the CDW to the disordered phase belongs to the three-dimensional (3D) Ising universality class, as found in other models of Rydberg arrays [54,55].

By contrast, the ordered phase at  $J' < J$  has a subextensive ground-state degeneracy which is robust against quantum fluctuations induced by a weak transverse field. To see this, note that the low-lying gapped excitations in this regime are domain walls created in pairs by applying a string operator on a given chain  $\ell$ ,

$$S_\ell(m_1, m_2) = \prod_{m_1 \leq m < m_2} X_{m,\ell}, \quad (5)$$

where  $m_1$  and  $m_2$  are the ends of the string. Two states in the ground-state manifold can be coupled only by nonlocal processes that move domain walls around the system, described by closed strings  $S_\ell(m_1, m_1 + L_\ell)$  with length  $L_\ell$ . The action of this operator corresponds to “sliding” the spin configuration along the chain direction [see Fig. 2(b)]. Moreover, the domain walls in the subspace of low-lying excited states behave as lineons, as their motion is restricted to the chain direction,

with dispersion

$$E_{\text{dw}}(k) = 2J - 2h_x \cos(ka) + O(h_x^2). \quad (6)$$

The motion of domain walls discussed here is reminiscent of the sliding transformation in the quantum Hall smectic phase [12].

Formally, the 1D nature of the excitation spectrum can be linked to an emergent symmetry inherited from the decoupled chains. Consider the action of a translation in the  $\ell$ th chain,

$$\mathcal{T}_\ell : Z_{m,\ell} \mapsto Z_{m+1,\ell}, \quad X_{m,\ell} \mapsto X_{m+1,\ell}. \quad (7)$$

This is not an exact symmetry since it does not commute with the Hamiltonian in the presence of interchain couplings. However, an emergent symmetry can be defined by the condition [13]

$$[H, \mathcal{P}\mathcal{T}_\ell\mathcal{P}] = 0, \quad (8)$$

where  $\mathcal{P}$  is a projector onto a low-energy subspace. Both the ground-state and two-domain-wall subspaces are stabilized under the action of the group generated by  $\mathcal{T}_\ell$ . This means that the faithful symmetry action at low energies is given by  $\mathbb{Z}_2^{L_x} \times \mathbb{Z}_2^{L_y}$ , yielding the  $2^{L_x+L_y}$  degenerate ground states. This exponential dependence on the linear size is characteristic of fracton models [5,6], which motivates us to call this the fCDW phase. This symmetry argument holds provided that the domain-wall pairs are gapped and the low-energy subspaces are clearly separated from multiparticle continua. However, the domain walls eventually condense as we increase the transverse field, driving a transition to the disordered phase. In the following we would like to understand the fate of the emergent symmetry near this critical point.

#### IV. EFFECTIVE FIELD THEORY

We now move to construct and analyze an effective theory for the transition between the fCDW and the disordered phase.

##### A. Continuum limit

We begin by putting all the chains at criticality in the uncoupled regime, i.e., near the point represented by a square in Fig. 2(a). Each critical chain is described by an Ising CFT [51]. This theory contains two classes of nontrivial primary operators: the energy operator  $\varepsilon$  with conformal dimensions  $(\frac{1}{2}, \frac{1}{2})$  and the spin field operator  $\sigma$ , with dimensions  $(\frac{1}{16}, \frac{1}{16})$  [56]. Lattice operators can be expanded as

$$X_{m,\ell} \sim \langle X_{m,\ell} \rangle \mathbb{I} + c_\sigma^X (-1)^m \sigma_\ell(x) + c_\varepsilon^X \varepsilon_\ell(x) + \dots, \quad (9)$$

$$Z_{m,\ell} \sim \langle Z_{m,\ell} \rangle \mathbb{I} + c_\sigma^Z (-1)^m \sigma_\ell(x) + c_\varepsilon^Z \varepsilon_\ell(x) + \dots, \quad (10)$$

where  $\mathbb{I}$  is the identity,  $x = ma$  is the position along the chain,  $c_\sigma^{X,Z}$  and  $c_\varepsilon^{X,Z}$  are nonuniversal real constants, and we omit higher-dimension operators. The  $\mathbb{Z}_2$  symmetry of the Ising CFT corresponds to the 1D translation, under which the spin field  $\sigma_\ell$  changes sign.

The low-energy Hamiltonian for decoupled chains can be written in terms of Majorana fermions. For a single chain, the holomorphic and antiholomorphic parts of the stress tensor are

given by

$$T(x) = \frac{i}{2} \eta \partial_x \eta, \quad \bar{T}(x) = -\frac{i}{2} \bar{\eta} \partial_x \bar{\eta}, \quad (11)$$

where  $\eta(x)$  and  $\bar{\eta}(x)$  are chiral Majorana fermions. The 1D Hamiltonian for a single chain near criticality is

$$H_{1D} = \int dx [v(T + \bar{T}) + m\varepsilon], \quad (12)$$

where  $v$  is the spin velocity and the energy operator  $\varepsilon(x) = i\bar{\eta}\eta(x)$  appears in the mass term. Tuning to the critical point, we set  $m = 0$ . Summing over all chains, we have

$$H_0 \simeq \sum_{\lambda \in \{h,v\}} \sum_{\ell_\lambda=1}^{L_\lambda} \int dx_\lambda v(T_{\lambda,\ell_\lambda} + \bar{T}_{\lambda,\ell_\lambda})(x_\lambda), \quad (13)$$

where we separate the contributions from horizontal (h) and vertical (v) chains by defining the labels  $\ell_h \in \{1, \dots, L_h \equiv L_y\}$ ,  $\ell_v \in \{1, \dots, L_v \equiv L_x\}$ , and the coordinates  $x_h = x$  and  $x_v = y$ .

Next, we add interchain couplings. Note that the interaction at a crossing has the form  $J'(Z_{m,\ell} + Z_{m+1,\ell})(Z_{m',\ell'} + Z_{m'+1,\ell'})$ . In the continuum limit, this interaction selects the nonoscillating terms in Eq. (10). We obtain

$$\delta H = \frac{vg}{2\pi} \sum_{k=1}^{N_c} \varepsilon_{h,\ell_h^k}(x_k) \varepsilon_{v,\ell_v^k}(y_k), \quad (14)$$

where  $\mathbf{x}_k = (x_k, y_k)$  are the positions of the crossings, which form a square lattice with spacing  $d_{\parallel}$ , the index  $\ell_{h,v}^k$  labels the horizontal and vertical chains which participate in the  $k$ th crossing, and  $N_c = L_x L_y$  is the total number of crossings. The coupling constant  $g$  is of order  $J'/J$ . We note that the interchain coupling also generates a mass term, but we can tune the mass to zero again by adjusting the longitudinal field.

The Hamiltonian is invariant under a discrete translational symmetry, which acts on local operators in the Ising CFT as

$$\begin{aligned} T_x : O_{v,\ell}(y) &\mapsto O_{v,\ell+1}(y), \\ O_{h,\ell}(x) &\mapsto O_{h,\ell}(x + d_{\parallel}); \end{aligned} \quad (15)$$

$$\begin{aligned} T_y : O_{h,\ell}(x) &\mapsto O_{h,\ell+1}(x), \\ O_{v,\ell}(y) &\mapsto O_{v,\ell}(y + d_{\parallel}). \end{aligned} \quad (16)$$

The interaction in Eq. (14) perturbs the critical chains with a macroscopic number of defects. To deal with this interaction, we take a second continuum limit equivalent to sending  $d_{\parallel} \rightarrow 0$ , appropriate when the length scales of the observables being probed are considerably larger than  $d_{\parallel}$ . The continuum limit of local operators is defined as  $O_{h,\ell_h}(x) \rightarrow d_{\parallel} O_h(x, d_{\parallel} \ell_h)$  and  $O_{v,\ell_v}(y) \rightarrow d_{\parallel} O_v(d_{\parallel} \ell_v, y)$ . The sums over the chains are replaced by integrals:

$$\sum_{\ell_\lambda=1}^{L_\lambda} (\dots) \rightarrow \int \frac{d\bar{x}_\lambda}{d_{\parallel}} (\dots), \quad \lambda \in \{h, v\} \quad (17)$$

where  $\bar{x}_h = x_v = y$  and  $\bar{x}_v = x_h = x$  correspond to the directions perpendicular to horizontal and vertical chains,

respectively. The effective Hamiltonian is then given by

$$H \simeq \int d^2\mathbf{x} v \left[ \sum_{\lambda \in \{h,v\}} (T_\lambda + \bar{T}_\lambda)(\mathbf{x}) + \frac{g}{2\pi} \varepsilon_h \varepsilon_v(\mathbf{x}) \right], \quad (18)$$

where  $d^2\mathbf{x} = dx dy$ .

To properly define a 2D field theory, we need to specify the corresponding operator product expansions. First, let us take the limit  $g \rightarrow 0$ , in which case the fields in Eq. (18) act as coarse-grained versions of the operators in the Ising CFT. Before we take the  $d_{\parallel} \rightarrow 0$  limit, the two-point functions of the nontrivial primaries read as

$$\langle \sigma_{\lambda,\ell_\lambda}(\mathbf{r}_\lambda) \sigma_{\lambda,\ell'_\lambda}(\mathbf{0}) \rangle_0 = \frac{\delta_{\ell_\lambda,\ell'_\lambda}}{|\mathbf{r}_\lambda|^{1/4}}, \quad (19)$$

$$\langle \varepsilon_{\lambda,\ell_\lambda}(\mathbf{r}_\lambda) \varepsilon_{\lambda,\ell'_\lambda}(\mathbf{0}) \rangle_0 = \frac{\delta_{\ell_\lambda,\ell'_\lambda}}{|\mathbf{r}_\lambda|^2}, \quad \lambda \in \{h, v\} \quad (20)$$

where  $\mathbf{r}_h = (x, v\tau)$  and  $\mathbf{r}_v = (y, v\tau)$  are coordinates in the (1+1)-dimensional Euclidean space-time with imaginary time  $\tau$ . All correlators of the form  $\langle O_h O_v \rangle_0$  vanish. We then take the second continuum limit, defining  $\mathbf{R} = (x, y, v\tau)$  and replacing  $\delta_{\ell_\lambda,\ell'_\lambda} \rightarrow \delta(d_{\parallel} \ell_\lambda - d_{\parallel} \ell'_\lambda)$ . Now, the same correlation functions written in the (2+1)-dimensional theory become

$$\langle \sigma_\lambda(\mathbf{R}) \sigma_\lambda(\mathbf{0}) \rangle = \frac{f_\lambda(x, y)}{|\mathbf{R}|^{1/4}}, \quad (21)$$

$$\langle \varepsilon_\lambda(\mathbf{R}) \varepsilon_\lambda(\mathbf{0}) \rangle = \frac{f_\lambda(x, y)}{|\mathbf{R}|^2}, \quad \lambda \in \{h, v\} \quad (22)$$

where  $f_h(x, y) = \delta(y)$  and  $f_v(x, y) = \delta(x)$ . Similar anisotropic correlators arise in theories of sliding Luttinger liquids [57,58]. To recover the 1D behavior of intrachain correlators, we must regularize the delta function at short distances as  $\delta(0) \rightarrow \frac{1}{d_{\parallel}}$ . Higher-point functions or correlators of other local operators (say, involving descendants or the stress-energy tensor) can be similarly regularized. This procedure perturbatively defines the 2D theory in Eq. (18).

## B. Emergent symmetries

The peculiar low-energy Hamiltonian in Eq. (18) inherits symmetries and dualities from the Ising chains. In the CFT, these symmetries are implemented by topological defect line operators labeled by the primary fields [59,60]. First, there is a Kramers-Wannier duality implemented by  $D^\sigma = \otimes_\ell D_\ell^\sigma$ , where  $D_\ell^\sigma$  is the  $\sigma$  defect of the  $\ell$ th chain [59]. The action of  $D^\sigma$  takes  $\varepsilon_\ell \mapsto -\varepsilon_\ell$ , exchanging the correlators of the fCDW and the disordered phase, and becomes a global symmetry at the critical point. Second and more interestingly, the emergent  $\mathbb{Z}_2^{L_x} \times \mathbb{Z}_2^{L_y}$  symmetry is manifested as the  $\varepsilon$  defect, which acts on horizontal chains as

$$D_{\ell_h}^\varepsilon \sigma_h(x, \ell_h a) = -\sigma_h(x, \ell_h a) D_{\ell_h}^\varepsilon, \quad (23)$$

and similarly for vertical chains. If we allowed for direct couplings between the order parameters of parallel chains, the symmetry would be lowered to a global  $\mathbb{Z}_2$  symmetry.

The defect line operators form the following fusion algebra [59]:

$$D_\ell^\varepsilon \times D_\ell^\varepsilon = 1, \quad (24)$$

$$D_\ell^\varepsilon \times D^\sigma = D^\sigma \times D_\ell^\varepsilon = D^\sigma, \quad (25)$$

$$D^\sigma \times D^\sigma = \bigotimes_{\ell=1}^{L_x+L_y} (1 + D_\ell^\varepsilon). \quad (26)$$

Here,  $\times$  denotes the fusion,  $\otimes$  takes the tensor product of symmetry lines on different chains, and we omit the trivial fusion rules involving the identity line defect. A similar version of this algebra was recently discussed in Ref. [61] on the lattice, as an example of a noninvertible subsystem symmetry. However, in our case, the algebra is simpler, descending from symmetries of decoupled chains. It is a noninvertible symmetry since the action of the Kramers-Wannier defect does not admit an inverse. It is known that the existence of such operators strongly constrains the low-energy spectrum [62]: For example, the existence of such line operators imposes that the Hilbert space of a perturbed 1+1 CFT cannot be trivially gapped [60]. This argument can be adapted to our realization since the algebra comes from a tensor product of CFTs, when the total number of chains  $L_x + L_y$  is odd (see Appendix A). Thus, we have the guarantee that the model defined by Eq. (18) cannot have a trivial ground state even at strong coupling.

### C. Perturbative RG analysis

We proceed to analyze the model perturbatively at weak coupling  $g \ll 1$ , corresponding to  $J' \ll J$ . The fate of the theory relies on the RG flow of the effective coupling  $g(s)$  at length scale  $s$  [63]. Power counting based on the correlator in Eq. (22) indicates that the coupling has effective scaling dimension  $\Delta = 3$  and is marginal at tree level. We calculate the beta function  $\beta(g)$  to leading order using the lattice spacing  $a$  as a short-distance cutoff and introducing the large-distance cutoffs  $D_x$  and  $D_y$  for the  $x$  and  $y$  directions (see Appendix B). The leading contribution appears at two-loop level and is strongly affected by the 1D nature of the correlators. We find that  $g$  behaves as a marginally irrelevant coupling, with beta function

$$\frac{dg}{dl} = -\ln\left(\frac{D_x D_y}{a^2}\right) g^3 + \dots, \quad (27)$$

where  $l = \ln(s/a)$  in the regime  $a \ll s \ll \min(D_x, D_y)$ .

Remarkably, the beta function depends explicitly on the ratio between the infrared and ultraviolet cutoffs, as found in models with UV-IR mixing [35,39]. Physically, we expect the scales  $D_x$  and  $D_y$  to be of the order of the linear system size in the  $x$  and  $y$  directions, respectively. For  $D_{x,y} \sim L_{x,y} a$ , the coefficient in Eq. (27) is proportional to  $\ln(N_c)$ , with  $N_c \gg 1$  being the number of crossings. Here we adopt the perspective that experiments with Rydberg atoms must be performed on a finite system where  $\ln(N_c)$  is a constant of order 1, but there are notorious subtleties in taking the continuum and thermodynamic limits in the presence of UV-IR mixing (see Refs. [15,40]).

Since the effective interchain coupling decreases at low energies, correlation functions can be calculated by perturbation theory. In particular, the leading contribution to correlators of crossed chains comes from the interaction at their crossing. Consider, for instance, the equal-time correlator for the energy

operator in a pair of horizontal and vertical chains. Taking a position  $x$  along the  $\ell_h = 0$  horizontal chain and position  $y$  along the  $\ell_v = 0$  chain, we obtain to first order in  $g$

$$\langle \varepsilon_h(x, 0) \varepsilon_v(0, y) \rangle \simeq -\frac{g}{2\pi} \int d^3\mathbf{R} \langle \varepsilon_h(x, 0) \varepsilon_h(\mathbf{R}) \rangle_0 \times \langle \varepsilon_v(0, y) \varepsilon_v(\mathbf{R}) \rangle_0. \quad (28)$$

Using the intrachain correlator in Eq. (22) and integrating over the spatial and temporal coordinates, we obtain

$$\langle \varepsilon_h(x, 0) \varepsilon_v(0, y) \rangle \sim -\frac{g}{2(x^2|y| + |x|y^2)} + O(g^3). \quad (29)$$

Note the unusual spatially anisotropic power-law decay, a prominent feature of fractonic behavior [34]. The homogeneous function of degree 3 in the denominator is consistent with the energy operator having an effective scaling dimension  $\Delta_\varepsilon = \frac{3}{2}$  in the (2+1)-dimensional theory, as expected from Eq. (22). However, the correlator is singular for  $x \rightarrow 0$  or  $y \rightarrow 0$ , which corresponds to taking two points on the same chain. When one of the coordinates is of the order of the lattice spacing, say  $x \sim a$ , we recover the correlator of the Ising CFT by  $\langle \varepsilon_h(a, 0) \varepsilon_v(0, y) \rangle \sim 1/y^2$  for  $|y| \gg a$ . The result in Eq. (29) captures the long-distance behavior of the correlation for the operator  $Z_{j,\ell} + Z_{j+1,\ell}$ , which can be measured by means of snapshots of the atomic states in Rydberg arrays [42,43].

### V. MAJORANA MEAN-FIELD THEORY

The perturbative RG analysis indicates that the fixed point of decoupled chains,  $g = 0$ , is stable against the interchain coupling. To test this picture, we study a lattice model that reduces to Eq. (18) in the continuum limit but also regularizes the short-distance behavior. We consider the effective Hamiltonian

$$\tilde{H} = \sum_{\ell,m} (J_e \tilde{Z}_{m,\ell} \tilde{Z}_{m+1,\ell} + h_e \tilde{X}_{m,\ell}) + J'_e \sum_{\diamond} \sum_{(i,j) \in \diamond} \tilde{X}_i \tilde{X}_j, \quad (30)$$

where the parameters  $J_e$ ,  $h_e$ , and  $J'_e$  can be chosen so as to tune to the critical point and to match  $v$  and  $g$  in the continuum limit. We denote the new Pauli operators by  $\tilde{X}_i$  and  $\tilde{Z}_i$  to avoid confusion with the original lattice model. One advantage of Eq. (30) over the original model is that the 1D symmetry is now manifest and onsite. This symmetry can be implemented by applying  $\prod_{m=1}^{L_\ell} \tilde{X}_{m,\ell}$ , which takes  $\tilde{Z}_{m,\ell} \mapsto -\tilde{Z}_{m,\ell}$  for all sites that belong to a given chain  $\ell$ .

Moreover, we can perform a generalized Jordan-Wigner transformation [3] and map the intrachain terms of Eq. (30) onto a stack of crossed Kitaev chains [64], in close connection with the Majorana representation in the field theory. We introduce two Majorana fermions at each site so that

$$\tilde{X}_{m,\ell} \mapsto i\gamma_{m,\ell}^0 \gamma_{m,\ell}^1, \quad (31)$$

with the anticommutation relation  $\{\gamma_{m,\ell}^b, \gamma_{m',\ell'}^{b'}\} = 2\delta^{bb'} \delta_{m,m'} \delta_{\ell,\ell'}$ . The other components of the local spin operator are written as

$$\tilde{Y}_{m,\ell} = \eta_\ell B_{m,\ell} \gamma_{m,\ell}^0, \quad (32)$$

$$\tilde{Z}_{m,\ell} = \eta_\ell B_{m,\ell} \gamma_{m,\ell}^1. \quad (33)$$

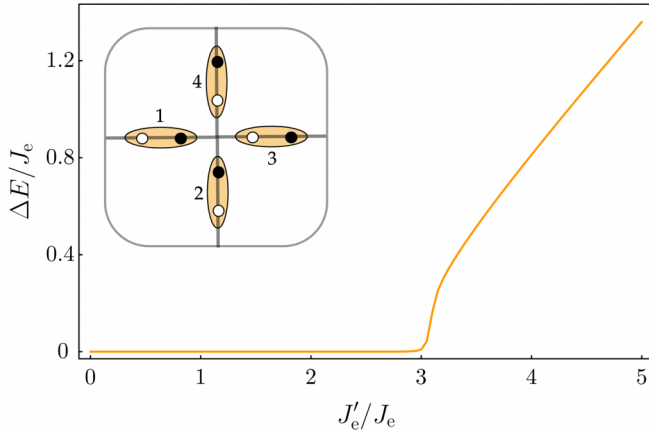


FIG. 3. Energy gap for Majorana fermion excitations calculated by solving the mean-field equations for the model in Eqs. (30) and (35) with  $h_e = J_e$  tuned to the critical point of the Ising chains. Here we focus on the lattice with  $\nu = 2$ . The vanishing gap at weak coupling is expected for a fixed point of decoupled chains. Inset: unit cell with eight Majorana modes  $\gamma_{\mathbf{R},\alpha}^a$ . Each site  $\alpha \in \{1, 2, 3, 4\}$  contains two modes,  $b \in \{0, 1\}$ , represented by white and black dots, respectively.

To ensure the Pauli algebra of physical operators, we have introduced the string operators

$$B_{m,\ell} = \prod_{m' \leq m} i\gamma_{m',\ell}^0 \gamma_{m',\ell}^1, \quad (34)$$

and the chain-dependent Klein factors  $\eta_\ell$  [65] that obey  $\{\eta_\ell, \eta_{\ell'}\} = 2\delta_{\ell,\ell'}$  and commute with the “dynamical” Majorana modes  $\gamma_{m,\ell}^b$ . The Hamiltonian is written in terms of Majorana fermions as

$$\begin{aligned} \tilde{H} = & \sum_{\ell,m} (iJ_e \gamma_{m,\ell}^1 \gamma_{m+1,\ell}^0 + ih_e \gamma_{m,\ell}^0 \gamma_{m,\ell}^1) \\ & - J'_e \sum_{\diamond} \sum_{(i,j) \in \diamond} \gamma_i^0 \gamma_i^1 \gamma_j^0 \gamma_j^1. \end{aligned} \quad (35)$$

The unit cell for the effective Majorana model on the  $\nu = 2$  lattice is shown in the inset of Fig. 3. We denote the eight Majoranas within each unit cell by  $\gamma_{\mathbf{R},\alpha}^b$ , where  $b \in \{0, 1\}$ ,  $\mathbf{R}$  is the position of the unit cell, and  $\alpha \in \{1, 2, 3, 4\}$  labels the sites around the crossing. The symmetries act projectively due to the gauged fermion parity. Time reversal conjugates complex numbers and takes  $\gamma_{\mathbf{R},\alpha}^b \mapsto (-1)^{b+1} \gamma_{\mathbf{R},\alpha}^b$ , while the  $C_4$  symmetry acts as  $\gamma_{\mathbf{R},\alpha}^b \mapsto \gamma_{\mathbf{R}',\alpha+1}^b$ , where  $b' = b + \cos^2(\frac{\pi\alpha}{2}) \pmod{2}$  and  $\mathbf{R}'$  is the rotated position.

We treat the quartic interaction in the fermionic representation of Eq. (35) using a Majorana mean-field approach [46,66,67]. In this approach, a departure from the decoupled-chain fixed point is signaled by a spontaneous hybridization between modes in perpendicular chains. We assume that the mean-field ansatz at criticality respects time-reversal invariance because this symmetry is preserved both in the fCDW and in the disordered phase. Imposing time-reversal as well as translation invariance, we obtain eight mean-field parameters allowed by symmetry:

$$A_\alpha = \langle i\gamma_{\mathbf{R},\alpha}^0 \gamma_{\mathbf{R},\alpha+1}^1 \rangle, \quad B_\alpha = \langle i\gamma_{\mathbf{R},\alpha}^1 \gamma_{\mathbf{R},\alpha+1}^0 \rangle. \quad (36)$$

Note that the mean-field decoupling of the interaction also generates the onsite amplitudes  $\langle i\gamma_{\mathbf{R},\alpha}^0 \gamma_{\mathbf{R},\alpha}^1 \rangle$ , but the latter can be absorbed into a renormalization of the transverse field  $h_e$ , which must be tuned to the critical point.

We diagonalize the quadratic mean-field Hamiltonian and solve the self-consistency equations numerically (see Appendix C for details). For  $h_e = J_e$  and small  $J'_e$ , we find that both  $A_\alpha$  and  $B_\alpha$  vanish and the fermionic spectrum is equivalent to critical Kitaev chains. As a consequence, the Majorana fermions are restricted to move within the respective chains. As we increase  $J'_e$ , the hybridization parameters eventually become nonzero and the 2D system develops an energy gap (see Fig. 3). In this regime, the  $C_4$  symmetry is spontaneously broken. Note, however, that the gapped regime occurs at strong coupling  $J'_e > J_e$ , where the connection with the original model via the effective field theory in Eq. (18) breaks down. While we cannot rule out additional phases around the tricritical point in Fig. 2(a), the mean-field theory confirms that the transition at weak to intermediate coupling is governed by the decoupled-chain fixed point. As characteristic of subdimensional criticality, at this fixed point we obtain further emergent 1D symmetries. In the effective field theory with  $g \rightarrow 0$ , the symmetry associated with the Kramers-Wannier defect  $D^\sigma$  is enlarged, and the resulting symmetries are generated by both  $D_\ell^\sigma$  and  $D_\ell^\epsilon$  for each chain.

## VI. CONCLUSIONS

We proposed a model for a fractonic quantum phase transition in Rydberg arrays. The setup consists of two layers of Rydberg chains in which the dominant interchain coupling occurs between pairs of perpendicular chains. If we neglect interactions between parallel chains, the ordered phase at weak coupling corresponds to a fCDW phase whose ground-state degeneracy increases exponentially with the number of chains or with the linear system size.

Starting from the fCDW phase and increasing the quantum fluctuations, we cross a transition to a disordered phase. We studied the critical point using an effective field theory in 2+1 dimensions that inherits properties of the Ising CFT. We also constructed a Majorana mean-field approach for a lattice model that reduces to the same field theory in the continuum limit. Our analysis shows that the critical point exhibits particles with restricted mobility, emergent symmetries, and anisotropic correlators that manifest the UV-IR mixing.

Moving forward, it would be interesting to explore nonequilibrium dynamics near criticality, extensions to  $\mathbb{Z}_n$ -ordered phases [50], and to apply numerical methods [68,69] to study the fCDW phase and the associated transitions. Our work represents a significant step towards the realization of fractonlike physics in quantum simulation platforms.

## ACKNOWLEDGMENTS

We acknowledge funding by Brazilian agencies Coordenação de Aperfeiçoamento de Pessoal de Nível Superior (R.A.M.) and Conselho Nacional de Desenvolvimento Científico e Tecnológico (R.G.P.). This work was supported by a grant from the Simons Foundation (Grant No. 1023171,

R.G.P.). Research at IIP-UFRN is supported by Brazilian ministries MEC and MCTI.

### APPENDIX A: NONINVERTIBLE EMERGENT SYMMETRY AND NONTRIVIALITY OF THE GROUND STATE

We will argue that the noninvertible symmetry implies a nontrivial ground state for an odd number of chains. As discussed in the main text, there is a  $\mathbb{Z}_2^{L_x} \times \mathbb{Z}_2^{L_y}$  symmetry generated by the line operators  $\{D_\ell^\varepsilon\}_{\ell=1}^{L_x+L_y}$  and a noninvertible symmetry generated by a Kramers-Wannier line  $D^\sigma$  at low energies for  $g \neq 0$ . We note that the fusion rules in Eqs. (24)–(26) depend on the number of chains, and therefore are not well defined in the thermodynamic limit. Similar behavior has been observed in the construction of the Kramers-Wannier defect (and the corresponding algebra with the  $\mathbb{Z}_2$  symmetry) in the transverse-field Ising chain [62] and in a related lattice model [61].

The expectation values of line operators are invariant under the RG flow. The reason is as follows. Given a vacuum  $|\Omega\rangle$ , we define the quantum dimensions

$$d^\sigma \equiv \langle D^\sigma \rangle = \langle \Omega | D^\sigma | \Omega \rangle, \quad (\text{A1})$$

$$d_S^\varepsilon \equiv \langle \otimes_{\ell \in S} D_\ell^\varepsilon \rangle = \langle \Omega | \otimes_{\ell \in S} D_\ell^\varepsilon | \Omega \rangle, \quad (\text{A2})$$

for any subset  $S$  of the total set of chains. It follows from the fusion ring that  $\{d^\sigma, \{d_S^\varepsilon\}\}$  satisfy polynomial equations with integer coefficients. Therefore, they must be RG invariants. This is completely analogous to the argument made in Ref. [60] in the context of (1 + 1)-dimensional QFTs.

First, for  $g = 0$ , consider the  $(\text{Ising})^{\otimes(L_x+L_y)}$  theory. By radial quantization, the ground state of this theory is  $|\Omega_0\rangle \equiv \otimes_{\ell=1}^{L_x+L_y} |1\rangle_\ell$ , where  $|1\rangle_\ell$  is the state corresponding to the identity operator of the  $\ell$ th chain. It is also known that the Kramers-Wannier defect has a quantum dimension of  $\sqrt{2}$  since  $D_\ell^\sigma |1\rangle_\ell = \sqrt{2} |1\rangle_\ell$ . Therefore,

$$D^\sigma |\Omega_0\rangle \equiv \langle D^\sigma \rangle_0 |\Omega_0\rangle = 2^{(L_x+L_y)/2} |\Omega_0\rangle. \quad (\text{A3})$$

Thus, even for  $g \neq 0$ , we have  $d^\sigma = \langle D^\sigma \rangle = \langle D^\sigma \rangle_0 = 2^{(L_x+L_y)/2}$  by the arguments above.

Suppose now that there is a unique ground state in the infrared described by a Hilbert space  $\mathcal{H}_{\text{IR}}$  such that  $\dim(\mathcal{H}_{\text{IR}}) = 1$ . In this case,

$$d^\sigma = \langle D^\sigma \rangle = \text{tr}_{\mathcal{H}_{\text{IR}}}(D^\sigma). \quad (\text{A4})$$

Physically, we can understand this equation in the path-integral approach where the trace corresponds to taking periodic boundary conditions in the time direction. Thus,  $d^\sigma$  computes the expectation value of  $D^\sigma$  on a time slice. The same amplitude can be computed by inserting the mesh in the time direction. In the path-integral picture, this works by slicing the Euclidean time direction into either  $T = \Delta_x \tau L_x$  or  $T = \Delta_y \tau L_y$ , depending on whether the mesh is positioned in the  $x$  or  $y$  direction, making the action of  $D^\sigma$  well defined (see Fig. 4).

As a consequence, one can interpret the quantization of  $d^\sigma$  as counting the dimension of a twisted Hilbert space  $\mathcal{H}_{D^\sigma}$ , where the operators (and corresponding states) have twisted

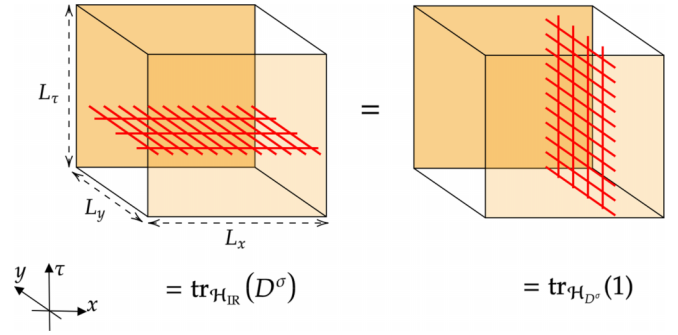


FIG. 4. Two ways of inserting the Kramers-Wannier defect  $D^\sigma$  in the path integral. On the left, the defect is defined on a constant-time slice, and its expectation value is computed in the infrared state. On the right, the defect is placed along the time direction, on a constant- $x$  slice. In this case,  $L_\tau$  is taken such that  $L_\tau = L_x$  to compute the dimension of the Hilbert space of the defect. At low energies, the results should match.

boundary conditions with the action of  $D^\sigma$ . But this is the same as computing the corresponding quantum dimension:

$$d^\sigma = \langle D^\sigma \rangle = \text{tr}_{\mathcal{H}_{D^\sigma}}(1), \quad (\text{A5})$$

leading to a contradiction for  $L_x + L_y$  odd, since the right-hand side is a non-negative integer and the left-hand side is not. Therefore, the infrared Hilbert space must have more than one state.

### APPENDIX B: DERIVATION OF THE RG EQUATION

We now derive the beta function for the coupling constant in the (2+1)-dimensional theory. Consider the partition function associated with the Hamiltonian in Eq. (18). The path integral can be written in terms of the free partition function  $Z_0$ , defined at  $g = 0$ , as

$$\begin{aligned} \frac{Z}{Z_0} &= \langle e^{-\frac{g}{2\pi} \int d^3\mathbf{R} \varepsilon_h \varepsilon_v(\mathbf{R})} \rangle_0 \\ &= 1 - gI^{(1)} + \frac{g^2}{2!} I^{(2)} - \frac{g^3}{3!} I^{(3)} + \dots, \end{aligned} \quad (\text{B1})$$

where  $d^3\mathbf{R} = dx dy d(v\tau)$  is the volume element in Euclidean space-time,  $\langle \dots \rangle_0$  denotes the expectation value in the free theory, and in the second line we expressed the ratio in a perturbative expansion. The corresponding integrals up to the third order are given by

$$\begin{aligned} I^{(1)} &= \frac{1}{2\pi} \int d^3\mathbf{R} \langle \varepsilon_h \varepsilon_v(\mathbf{R}) \rangle_0, \\ I^{(2)} &= \frac{1}{(2\pi)^2} \int d^3\mathbf{R}_1 d^3\mathbf{R}_2 \langle \varepsilon_h \varepsilon_v(\mathbf{R}_1) \varepsilon_h \varepsilon_v(\mathbf{R}_2) \rangle_0, \\ I^{(3)} &= \frac{1}{(2\pi)^3} \int d^3\mathbf{R}_1 d^3\mathbf{R}_2 d^3\mathbf{R}_3 \\ &\quad \times \langle \varepsilon_h \varepsilon_v(\mathbf{R}_1) \varepsilon_h \varepsilon_v(\mathbf{R}_2) \varepsilon_h \varepsilon_v(\mathbf{R}_3) \rangle_0. \end{aligned} \quad (\text{B2})$$

The integrals must be regularized by imposing a UV cutoff. We choose a specific cutoff scheme following the approach explained in Ref. [63]. The three steps behind the perturbative renormalization group are as follows: (1) perform an

infinitesimal RG transformation, where the short-distance cutoff  $a$  is renormalized as  $a \rightarrow a(1 + dl)$ , (2) discard all contributions which are  $O(dl^2)$  or higher; (3) impose that the partition function must remain invariant, reading off the corresponding renormalization conditions. This is the standard approach in the study of scale-invariant fixed points, but we will encounter difficulties related to UV-IR mixing when we perturb around the fixed point of decoupled crossed chains.

The first-order term is invariant under the scaling, implying that the perturbation is tree-level marginal as mentioned in the main text. The second-order term only contributes to the renormalization of irrelevant interactions, such as  $\varepsilon_h \partial_x \varepsilon_h$  and  $\varepsilon_v \partial_x \varepsilon_v$ . The renormalization of the coupling appears at third order or two-loop level. By Wick's theorem, the contribution in Eq. (B2) can be written as

$$I^{(3)} = \frac{3}{(2\pi)^3} \int d^3 \mathbf{R}_1 d^3 \mathbf{R}_2 d^3 \mathbf{R}_3 \langle \varepsilon_h(\mathbf{R}_1) \varepsilon_v(\mathbf{R}_3) \rangle_0 \times \langle \varepsilon_v(\mathbf{R}_1) \varepsilon_v(\mathbf{R}_2) \rangle_0 \langle \varepsilon_h(\mathbf{R}_2) \varepsilon_h(\mathbf{R}_3) \rangle_0 + (h \leftrightarrow v), \quad (\text{B3})$$

where the combinatorial factor comes from exchanging the positions of the interaction vertices. Taking the leading contributions as  $\mathbf{R}_3 \rightarrow \mathbf{R}_1$  and using the correlator for decoupled chains in Eq. (22), we obtain

$$I^{(3)} = \frac{6}{(2\pi)^3} \int d^3 \mathbf{R} \langle \varepsilon_h \varepsilon_v(\mathbf{R}) \rangle_0 \times \int \frac{dy_{12} d(v\tau_{12}) dx_{23} d(v\tau_{23})}{[y_{12}^2 + (v\tau_{12})^2][x_{23}^2 + (v\tau_{23})^2]}, \quad (\text{B4})$$

where  $\tau_{12} = \tau_1 - \tau_2$ ,  $\tau_{23} = \tau_2 - \tau_3$ ,  $x_{23} = x_2 - x_3$ , and  $y_{12} = y_1 - y_2$ . This is the point where the calculation departs from the standard scheme for conformally invariant fixed points. Note the anisotropic dependence of the integrand in the four-dimensional space spanned by  $(x_{12}, y_{23}, \tau_{12}, \tau_{23})$ . Since the integrand is singular for  $y_{12} = \tau_{12} = 0$  or  $x_{23} = \tau_{23} = 0$ , we cannot simply integrate out a spherical shell in the four-dimensional space. This dependence can be traced back to the 1D nature of the correlators at the decoupled-chain fixed point. We proceed by integrating out arbitrary time differences  $-\infty < \tau_{12}, \tau_{23} < \infty$ , while keeping a short-distance cutoff. We obtain

$$I^{(3)} = \frac{3}{4\pi} \int d^3 \mathbf{R}_1 \langle \varepsilon_h \varepsilon_v(\mathbf{R}) \rangle_0 \int_a^{D_y} \frac{dy_{12}}{|y_{12}|} \int_a^{D_x} \frac{dx_{23}}{|x_{23}|} = \frac{3}{\pi} \ln\left(\frac{D_x}{a}\right) \ln\left(\frac{D_y}{a}\right) I^{(1)}, \quad (\text{B5})$$

where we imposed both the spatial UV cutoff  $a$  and IR cutoffs  $D_x$  and  $D_y$ . Note the peculiar double-logarithmic dependence, which diverges for  $D_x \rightarrow \infty$  or  $D_y \rightarrow \infty$ . The scales  $D_x$  and  $D_y$  can be interpreted as being of the order of the linear system size in the  $x$  and  $y$  directions, respectively. As discussed in the context of UV-IR mixing in Bose-metal-like models [15,40], the result may depend on how we handle the thermodynamic limit along with the continuum limit.

We can now perform the renormalization steps on the term in Eq. (B5). Rescaling  $a \rightarrow a(1 + dl)$ , we obtain  $I^{(3)} \rightarrow$

$I^{(3)} + \delta I^{(3)} + O(dl^2)$ , where

$$\delta I^{(3)} = -6 \ln\left(\frac{D_x D_y}{a^2}\right) dl I^{(1)}. \quad (\text{B6})$$

The corresponding change in the perturbative expansion defined in Eq. (B1) can be written as

$$\frac{Z}{Z_0} = 1 - \frac{1}{2\pi} \left[ g - \ln\left(\frac{D_x D_y}{a^2}\right) g^3 dl \right] I^{(1)} + \frac{g^2}{2!} I^{(2)} - \frac{g^3}{3!} I^{(3)} + \dots, \quad (\text{B7})$$

where we neglected irrelevant terms stemming from  $I^{(2)}$ . Imposing invariance under the RG transformation, we see that the coupling is renormalized as  $g \rightarrow g + dg$ , which leads to the beta function in Eq. (27).

### APPENDIX C: MEAN-FIELD EQUATIONS

Here we discuss the diagonalization of the mean-field Hamiltonian and the derivation of the self-consistency equations.

We introduce momentum modes as

$$\gamma_{\mathbf{R},\alpha}^b = \sqrt{\frac{2}{N_c}} \sum_{\mathbf{k} \in \text{BZ}} e^{i\mathbf{k} \cdot \mathbf{R}} \gamma_{\mathbf{k},\alpha}^b, \quad (\text{C1})$$

where  $\text{BZ} \equiv [-\pi/d_{\parallel}, \pi/d_{\parallel}]^2$ , with  $d_{\parallel} = 2a$ , stands for the Brillouin zone of the square lattice with  $N_c = L_x L_y$  unit cells. For Majorana fermions, we have the relation  $\gamma_{\mathbf{k},\alpha}^b = (\gamma_{\mathbf{k},\alpha}^b)^\dagger$ , which allows us to restrict to modes in one half of the Brillouin zone, say  $\text{HBZ} \equiv [-\pi/d_{\parallel}, \pi/d_{\parallel}] \times [0, \pi/d_{\parallel}]$ . These complex fermion operators satisfy  $\{\gamma_{\mathbf{k},\alpha}^b, (\gamma_{\mathbf{k}',\alpha'}^b)^\dagger\} = \delta^{b b'} \delta_{\mathbf{k},\mathbf{k}'} \delta_{\alpha,\alpha'}$ .

The mean-field Hamiltonian can be cast in the form

$$\tilde{H}_{\text{MF}} = \sum_{\mathbf{k} \in \text{HBZ}} \Psi_{\mathbf{k}}^\dagger \mathcal{H}_{\text{MF}}(\mathbf{k}) \Psi_{\mathbf{k}}, \quad (\text{C2})$$

where  $\Psi_{\mathbf{k}} = (\gamma_{\mathbf{k},1}^0, \gamma_{\mathbf{k},2}^0, \dots, \gamma_{\mathbf{k},3}^1, \gamma_{\mathbf{k},4}^1)^T$  is an eight-component spinor and  $\mathcal{H}_{\text{MF}}(\mathbf{k})$  is an  $8 \times 8$  Hermitian matrix that depends on  $J_e, h_e, J'_e$ , as well as on the mean-field parameters defined in Eq. (36). These parameters are to be found by self-consistency. The amplitudes of interest have the form

$$\langle i\gamma_{\mathbf{R},\alpha}^b \gamma_{\mathbf{R},\alpha+1}^{b'} \rangle = \frac{1}{N_c} \sum_{\mathbf{k} \in \text{HBZ}} [(i\gamma_{\mathbf{k},\alpha}^b (\gamma_{\mathbf{k},\alpha+1}^{b'})^\dagger) + \text{c.c.}]. \quad (\text{C3})$$

We can find a unitary transformation  $U(\mathbf{k})$  such that  $U^\dagger(\mathbf{k}) \mathcal{H}_{\text{MF}}(\mathbf{k}) U(\mathbf{k}) = \text{diag}(\varepsilon_{\mathbf{k},1}, \varepsilon_{\mathbf{k},2}, \dots, \varepsilon_{\mathbf{k},8})$ . Then, the eigenspinors  $\tilde{\Psi}_{\mathbf{k}} \equiv (\tilde{\gamma}_{\mathbf{k},1}, \tilde{\gamma}_{\mathbf{k},2}, \dots, \tilde{\gamma}_{\mathbf{k},8})^T$  are such that  $\Psi_{\mathbf{k}} = U(\mathbf{k}) \tilde{\Psi}_{\mathbf{k}}$ . The mean-field ground state is constructed by occupying all single-particle states with negative energy. Using the band-filling condition  $\langle \tilde{\gamma}_{\mathbf{k},A} (\tilde{\gamma}_{\mathbf{k},B})^\dagger \rangle = \delta_{AB} \Theta(\varepsilon_{\mathbf{k},A}) \equiv T_{AB}(\mathbf{k})$  for  $A, B \in \{1, \dots, 8\}$ , where  $\Theta(x)$  is the Heaviside step function, we can rewrite Eq. (C3) in a compact form:

$$\langle i\gamma_{\mathbf{R},\alpha}^b \gamma_{\mathbf{R},\alpha+1}^{b'} \rangle = -\frac{2}{N_c} \sum_{\mathbf{k} \in \text{HBZ}} \text{tr}[T(\mathbf{k}) U^\dagger(\mathbf{k}) P_\alpha^{b b'} U(\mathbf{k})], \quad (\text{C4})$$



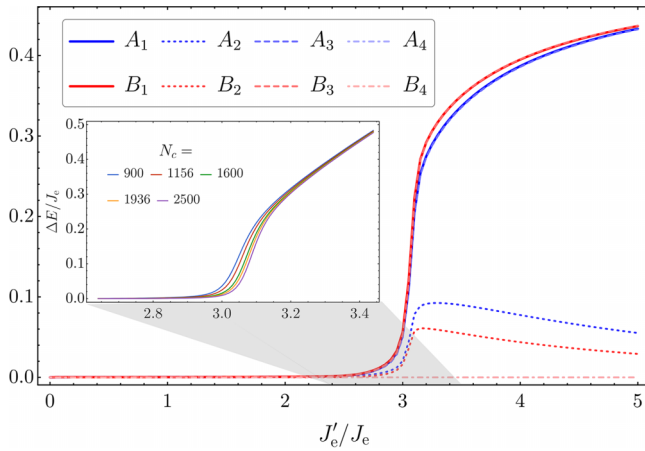


FIG. 5. Results from the mean-field theory. Solutions of the eight mean-field parameters in Eqs. (C5) and (C6), computed for  $N_c = 50 \times 50 = 2500$  unit cells. Note that the  $C_4$ -related parameters acquire different values for  $J'_e/J_e \gtrsim 3$ . Inset: Finite-size scaling of the energy gap around  $J'_e/J_e \simeq 3$ , evaluated from  $N_c = 900$  to 2500 unit cells.

where we define the projector  $P_\alpha^{b'b}$ , with components  $[P_\alpha^{b'b}]_{AB} = \delta_{A,\alpha+4(b-1)}\delta_{B,\alpha+4(b-1)}$ . Thus, the eight mean-field parameters must satisfy the following set of equations:

$$A_\alpha = -\frac{2}{N_c} \sum_{\mathbf{k} \in \text{HBZ}} \text{tr}[T(\mathbf{k})U^\dagger(\mathbf{k})P_\alpha^{10}U(\mathbf{k})], \quad (\text{C5})$$

$$B_\alpha = -\frac{2}{N_c} \sum_{\mathbf{k} \in \text{HBZ}} \text{tr}[T(\mathbf{k})U^\dagger(\mathbf{k})P_\alpha^{01}U(\mathbf{k})]. \quad (\text{C6})$$

Note that  $U(\mathbf{k})$  depends on  $A_\alpha$  and  $B_\alpha$ . We solved these equations numerically by standard iteration until convergence is reached.

For  $J_e \neq h_e$ , we find that the gap in both fCDW and disordered phases is stable under turning on the coupling  $J'_e$ , as expected. The result for the mean-field parameters at criticality,  $J'_e = J_e$ , is shown in Fig. 5. We see that  $A_\alpha$  and  $B_\alpha$  become nonzero only for a fairly strong interchain coupling  $J'_e/J_e \gtrsim 3$ . The solution with nonzero hybridization breaks  $C_4$  symmetry and the resulting fermionic spectrum is gapped. We have checked that finite-size effects are significant only near the critical coupling; see the inset in Fig. 5 for the behavior of the energy gap.

- [1] J. A. Hertz, Quantum critical phenomena, *Phys. Rev. B* **14**, 1165 (1976).
- [2] S. L. Sondhi, S. M. Girvin, J. P. Carini, and D. Shahar, Continuous quantum phase transitions, *Rev. Mod. Phys.* **69**, 315 (1997).
- [3] S. Sachdev, *Quantum Phase Transitions*, 2nd ed. (Cambridge University Press, Cambridge, 2011).
- [4] E. Fradkin, *Field Theories of Condensed Matter Physics* (Cambridge University Press, Cambridge, 2013).
- [5] R. M. Nandkishore and M. Hermele, Fractons, *Annu. Rev. Condens. Matter Phys.* **10**, 295 (2019).
- [6] M. Pretko, X. Chen, and Y. You, Fracton phases of matter, *Int. J. Mod. Phys. A* **35**, 2030003 (2020).
- [7] A. Gromov and L. Radzihovsky, *Colloquium: Fracton matter*, *Rev. Mod. Phys.* **96**, 011001 (2024).
- [8] C. Chamon, Quantum glassiness in strongly correlated clean systems: An example of topological overprotection, *Phys. Rev. Lett.* **94**, 040402 (2005).
- [9] S. Bravyi, B. Leemhuis, and B. M. Terhal, Topological order in an exactly solvable 3D spin model, *Ann. Phys.* **326**, 839 (2011).
- [10] J. Haah, Local stabilizer codes in three dimensions without string logical operators, *Phys. Rev. A* **83**, 042330 (2011).
- [11] S. Vijay, J. Haah, and L. Fu, Fracton topological order, generalized lattice gauge theory, and duality, *Phys. Rev. B* **94**, 235157 (2016).
- [12] M. J. Lawler and E. Fradkin, Quantum Hall smectics, sliding symmetry, and the renormalization group, *Phys. Rev. B* **70**, 165310 (2004).
- [13] Z. Nussinov and J. van den Brink, Compass models: Theory and physical motivations, *Rev. Mod. Phys.* **87**, 1 (2015).
- [14] Y. You, Z. Bi, and M. Pretko, Emergent fractons and algebraic quantum liquid from plaquette melting transitions, *Phys. Rev. Res.* **2**, 013162 (2020).
- [15] P. Gorantla, H. T. Lam, N. Seiberg, and S.-H. Shao, Low-energy limit of some exotic lattice theories and UV/IR mixing, *Phys. Rev. B* **104**, 235116 (2021).
- [16] M. Mühlhauser, M. R. Walther, D. A. Reiss, and K. P. Schmidt, Quantum robustness of fracton phases, *Phys. Rev. B* **101**, 054426 (2020).
- [17] T. F. J. Poon and X.-J. Liu, Quantum phase transition of fracton topological orders, *Phys. Rev. Res.* **3**, 043114 (2021).
- [18] G.-Y. Zhu, J.-Y. Chen, P. Ye, and S. Trebst, Topological fracton quantum phase transitions by tuning exact tensor network states, *Phys. Rev. Lett.* **130**, 216704 (2023).
- [19] E. Lake and M. Hermele, Subdimensional criticality: Condensation of lineons and planons in the X-cube model, *Phys. Rev. B* **104**, 165121 (2021).
- [20] B. C. Raychaudhuri and D. J. Williamson, Higher-form subsystem symmetry breaking: Subdimensional criticality and fracton phase transitions, *SciPost Phys.* **15**, 017 (2023).
- [21] K. Slagle and Y. B. Kim, Quantum field theory of X-cube fracton topological order and robust degeneracy from geometry, *Phys. Rev. B* **96**, 195139 (2017).
- [22] M. Pretko, The fracton gauge principle, *Phys. Rev. B* **98**, 115134 (2018).
- [23] D. Bulmash and M. Barkeshli, Higgs mechanism in higher-rank symmetric U(1) gauge theories, *Phys. Rev. B* **97**, 235112 (2018).
- [24] H. Ma, M. Hermele, and X. Chen, Fracton topological order from the Higgs and partial-confinement mechanisms of rank-two gauge theory, *Phys. Rev. B* **98**, 035111 (2018).
- [25] A. Gromov, Towards classification of fracton phases: The multipole algebra, *Phys. Rev. X* **9**, 031035 (2019).
- [26] Y. You, T. Devakul, S. L. Sondhi, and F. J. Burnell, Fractonic Chern-Simons and BF theories, *Phys. Rev. Res.* **2**, 023249 (2020).

- [27] N. Seiberg and S.-H. Shao, Exotic  $U(1)$  symmetries, duality, and fractons in 3+1-dimensional quantum field theory, *SciPost Phys.* **9**, 046 (2020).
- [28] K. Slagle, Foliated quantum field theory of fracton order, *Phys. Rev. Lett.* **126**, 101603 (2021).
- [29] W. B. Fontana, P. R. S. Gomes, and C. Chamon, Lattice Clifford fractons and their Chern-Simons-like theory, *SciPost Phys. Core* **4**, 012 (2021).
- [30] J. Sullivan, A. Dua, and M. Cheng, Fractonic topological phases from coupled wires, *Phys. Rev. Res.* **3**, 023123 (2021).
- [31] A. Paramekanti, L. Balents, and M. P. A. Fisher, Ring exchange, the exciton Bose liquid, and bosonization in two dimensions, *Phys. Rev. B* **66**, 054526 (2002).
- [32] N. Seiberg and S.-H. Shao, Exotic symmetries, duality, and fractons in 2+1-dimensional quantum field theory, *SciPost Phys.* **10**, 027 (2021).
- [33] Y. You, J. Bibo, F. Pollmann, and T. L. Hughes, Fracton critical point at a higher-order topological phase transition, *Phys. Rev. B* **106**, 235130 (2022).
- [34] Y. You and R. Moessner, Fractonic plaquette-dimer liquid beyond renormalization, *Phys. Rev. B* **106**, 115145 (2022).
- [35] K. T. Grosvenor, R. Lier, and P. Surówka, Fractonic Berezinskii-Kosterlitz-Thouless transition from a renormalization group perspective, *Phys. Rev. B* **107**, 045139 (2023).
- [36] Z.-X. Luo, R. C. Spieler, H.-Y. Sun, and A. Karch, Boundary theory of the X-cube model in the continuum, *Phys. Rev. B* **106**, 195102 (2022).
- [37] W. B. Fontana and R. G. Pereira, Boundary modes in the Chamon model, *SciPost Phys.* **15**, 010 (2023).
- [38] C. Xu and J. Moore, Reduction of effective dimensionality in lattice models of superconducting arrays and frustrated magnets, *Nucl. Phys. B* **716**, 487 (2005).
- [39] A. Kapustin, T. McKinney, and I. Z. Rothstein, Wilsonian effective field theory of two-dimensional Van Hove singularities, *Phys. Rev. B* **98**, 035122 (2018).
- [40] E. Lake, Renormalization group and stability in the exciton Bose liquid, *Phys. Rev. B* **105**, 075115 (2022).
- [41] A. Browaeys and T. Lahaye, Many-body physics with individually controlled Rydberg atoms, *Nat. Phys.* **16**, 132 (2020).
- [42] G. Semeghini, H. Levine, A. Keesling, S. Ebadi, T. T. Wang, D. Bluvstein, R. Verresen, H. Pichler, M. Kalinowski, R. Samajdar, A. Omran, S. Sachdev, A. Vishwanath, M. Greiner, V. Vuletić, and M. D. Lukin, Probing topological spin liquids on a programmable quantum simulator, *Science* **374**, 1242 (2021).
- [43] P. Scholl, M. Schuler, H. J. Williams, A. A. Eberharter, D. Barredo, K.-N. Schymik, V. Lienhard, L.-P. Henry, T. C. Lang, T. Lahaye, A. M. Läuchli, and A. Browaeys, Quantum simulation of 2D antiferromagnets with hundreds of Rydberg atoms, *Nature (London)* **595**, 233 (2021).
- [44] F. M. Surace, P. P. Mazza, G. Giudici, A. Lerose, A. Gambassi, and M. Dalmonte, Lattice gauge theories and string dynamics in Rydberg atom quantum simulators, *Phys. Rev. X* **10**, 021041 (2020).
- [45] R. Verresen, M. D. Lukin, and A. Vishwanath, Prediction of toric code topological order from Rydberg blockade, *Phys. Rev. X* **11**, 031005 (2021).
- [46] K. Slagle, Y. Liu, D. Aasen, H. Pichler, R. S. K. Mong, X. Chen, M. Endres, and J. Alicea, Quantum spin liquids bootstrapped from Ising criticality in Rydberg arrays, *Phys. Rev. B* **106**, 115122 (2022).
- [47] N. E. Myerson-Jain, S. Yan, D. Weld, and C. Xu, Construction of fractal order and phase transition with Rydberg atoms, *Phys. Rev. Lett.* **128**, 017601 (2022).
- [48] R. Samajdar, D. G. Joshi, Y. Teng, and S. Sachdev, Emergent  $\mathbb{Z}_2$  gauge theories and topological excitations in Rydberg atom arrays, *Phys. Rev. Lett.* **130**, 043601 (2023).
- [49] J. Y. Lee, J. Ramette, M. A. Metlitski, V. Vuletić, W. W. Ho, and S. Choi, Landau-forbidden quantum criticality in Rydberg quantum simulators, *Phys. Rev. Lett.* **131**, 083601 (2023).
- [50] P. Fendley, K. Sengupta, and S. Sachdev, Competing density-wave orders in a one-dimensional hard-boson model, *Phys. Rev. B* **69**, 075106 (2004).
- [51] K. Slagle, D. Aasen, H. Pichler, R. S. K. Mong, P. Fendley, X. Chen, M. Endres, and J. Alicea, Microscopic characterization of Ising conformal field theory in Rydberg chains, *Phys. Rev. B* **104**, 235109 (2021).
- [52] M. Saffman, T. G. Walker, and K. Mølmer, Quantum information with Rydberg atoms, *Rev. Mod. Phys.* **82**, 2313 (2010).
- [53] A. A. Ovchinnikov, D. V. Dmitriev, V. Y. Krivnov, and V. O. Cheranovskii, Antiferromagnetic Ising chain in a mixed transverse and longitudinal magnetic field, *Phys. Rev. B* **68**, 214406 (2003).
- [54] R. Samajdar, W. W. Ho, H. Pichler, M. D. Lukin, and S. Sachdev, Complex density wave orders and quantum phase transitions in a model of square-lattice Rydberg atom arrays, *Phys. Rev. Lett.* **124**, 103601 (2020).
- [55] S. Yang and J.-B. Xu, Density-wave-ordered phases of Rydberg atoms on a honeycomb lattice, *Phys. Rev. E* **106**, 034121 (2022).
- [56] P. Di Francesco, P. Mathieu, and D. Sénéchal, *Conformal Field Theory* (Springer, New York, 1996).
- [57] R. Mukhopadhyay, C. L. Kane, and T. C. Lubensky, Crossed sliding Luttinger liquid phase, *Phys. Rev. B* **63**, 081103(R) (2001).
- [58] O. A. Starykh, R. R. P. Singh, and G. C. Levine, Spinons in a crossed-chains model of a 2D spin liquid, *Phys. Rev. Lett.* **88**, 167203 (2002).
- [59] J. Fröhlich, J. Fuchs, I. Runkel, and C. Schweigert, Kramers-Wannier duality from conformal defects, *Phys. Rev. Lett.* **93**, 070601 (2004).
- [60] C.-M. Chang, Y.-H. Lin, S.-H. Shao, Y. Wang, and X. Yin, Topological defect lines and renormalization group flows in two dimensions, *J. High Energy Phys.* **01** (2019) 026.
- [61] W. Cao, L. Li, M. Yamazaki, and Y. Zheng, Subsystem non-invertible symmetry operators and defects, *SciPost Phys.* **15**, 155 (2023).
- [62] N. Seiberg, S. Seifnashri, and S.-H. Shao, Non-invertible symmetries and LSM-type constraints on a tensor product Hilbert space, *SciPost Phys.* **16**, 154 (2024).
- [63] J. Cardy, *Scaling and Renormalization in Statistical Physics* (Cambridge University Press, Cambridge, 1996).
- [64] A. Y. Kitaev, Unpaired Majorana fermions in quantum wires, *Phys. Usp.* **44**, 131 (2001).
- [65] N. Crampé and A. Trombettoni, Quantum spins on star graphs and the Kondo model, *Nucl. Phys. B* **871**, 526 (2013).
- [66] A. Rahmani and M. Franz, Interacting Majorana fermions, *Rep. Prog. Phys.* **82**, 084501 (2019).
- [67] J.-H. Chen, C. Mudry, C. Chamon, and A. M. Tsvelik, Model of spin liquids with and without time-reversal symmetry, *Phys. Rev. B* **99**, 184445 (2019).

- [68] R. Samajdar, W. W. Ho, H. Pichler, M. D. Lukin, and S. Sachdev, Quantum phases of Rydberg atoms on a kagome lattice, *Proc. Natl. Acad. Sci. USA* **118**, e2015785118 (2021).
- [69] E. Merali, I. J. S. D. Vlugt, and R. G. Melko, Stochastic series expansion quantum Monte Carlo for Rydberg arrays, *SciPost Phys. Core* **7**, 016 (2024).